

The White Dwarf Pareto: Tracing Mass Loss in Binary Systems

SAHAR SHAHAF 

*Department of Particle Physics and Astrophysics
Weizmann Institute of Science
Rehovot 7610001, Israel*

ABSTRACT

The white dwarf mass distribution has been studied primarily at two extremes: objects that presumably evolved as single stars and members of close binaries that likely underwent substantial interaction. This work considers the intermediate separation regime of ~ 1 au and demonstrates how binary interaction affects white dwarf masses. The binary mass ratio distribution is utilized for this purpose. Modeled as a truncated Pareto profile, this distribution provides insights into the populations' properties and evolutionary history. When applied to homogeneous samples of binaries with giant primaries of similar age, the distribution's shape constrains the fraction of white dwarf companions, the white dwarf mass distribution, and the properties of their progenitors. As a test case, this method is applied to a small spectroscopic sample of binaries in open clusters with red giant primaries and orbital periods between 0.5 and 20 years. The analysis reveals that white dwarfs in these systems are $\sim 20\%$ less massive than their isolated counterparts, with a typical mass of $\sim 0.55 M_{\odot}$. Their progenitors likely lost 80–85% of their mass, with binary interactions enhancing mass loss by an additional $\sim 0.2 M_{\odot}$. These findings highlight the utility of this approach for studying binary evolution and improving population models, particularly with future datasets from Gaia and other large-scale surveys.

Keywords: White dwarf stars (1799) — Red giant stars (1372) — Binary stars (154) — Spectroscopic binary stars (1557) — Mass ratio (1012) — Astrostatistics (1882)

1. INTRODUCTION

Stellar multiplicity is established during the early stages of star formation, with primordial configurations dynamically evolving to produce the observed populations of single, binary, and higher-order multiple systems (Larson 1972; Reipurth et al. 2014; Beuther et al. 2019; Rosen et al. 2020; Offner et al. 2023). Binary systems are particularly prevalent, comprising about half of all Sun-like stars, three-quarters of A-type stars, and nearly all B- and O-type stars (e.g., Raghavan et al. 2010; Duchêne & Kraus 2013; Offner et al. 2023). The high occurrence of binaries significantly influences various astrophysical processes, a fact recognized even before large samples became available, motivating early empirical studies of

binary populations over a century ago (e.g., van Biesbroeck 1916; Öpik 1924; Kuiper 1935).

Whether single or part of a binary system, all stars eventually exhaust their nuclear energy supplies, leaving behind stellar remnants, most commonly white dwarfs (Althaus et al. 2010). Despite the high frequency of white dwarfs, with hundreds of thousands already discovered either in binaries or isolation (Gentile Fusillo et al. 2021; Shahaf et al. 2024), key aspects of their population remain incompletely understood (e.g., Isern et al. 2022; Hallakoun et al. 2024). In particular, the relationship between a white dwarf's mass and that of its progenitor star, known as the initial-to-final mass relation, or the IFMR, remains an area of active research (Tremblay et al. 2016; Cummings et al. 2016, 2018; El-Badry et al. 2018; Cunningham et al. 2024; Hollands et al. 2024; Addari et al. 2024).

The extent to which binarity affects the mass of white dwarfs strongly depends on the orbital separation. At sufficiently large separations, the two stars are expected

to evolve independently (Barrientos & Chanamé 2021; Hollands et al. 2024; Heintz et al. 2022). However, at close separation, binary interaction plays an important role. It becomes evident when considering the population of extremely low-mass (e.g., Brown et al. 2010; Kosakowski et al. 2023), ultramassive (Cheng et al. 2020; Fleury et al. 2022; Kilic et al. 2023) or highly magnetized white dwarfs (Moss et al. 2023). However, a significant portion of the population presumably exists in neither of these extremities. Still, until recently, white dwarfs in binaries separated by ~ 1 au have eluded detection (Holberg et al. 2013).

This situation has changed with the recent data release by the Gaia spacecraft (El-Badry 2024; Tremblay et al. 2024). The astrometric and spectroscopic orbits from Gaia uncovered a large population of binaries comprised of a white dwarf and main sequence star at this intermediate separation regime (Shahaf et al. 2024; Yamaguchi et al. 2024a,b). Some of the emerging properties of this population already provided new insights and challenges to stellar and binary evolution models (Hallakoun et al. 2024; Shahaf et al. 2024; Yamaguchi et al. 2024a; Rekhi et al. 2024).

This work presents a method to estimate the white dwarf mass distribution and constrain the IFMR using binaries where the primary star is a red giant. A truncated power-law (i.e., a Pareto distribution) approximates the mass ratio distribution, whose properties are sensitive to the IFMR parameters. This approach can be applied to spectroscopic binary samples, allowing exploration across a wide range of orbital separations and offering new insights into binary and stellar evolution in regimes that have been previously underexplored.

The structure of the paper is as follows: Section 2 presents the expected shape of the mass ratio and modified mass function distributions; Section 3 applies this model, as a test case, to a spectroscopic sample of binaries with red giant primaries from open clusters. The results are discussed in Section 4. Section 5 summarizes the findings and outlines avenues for future study.

2. COMPANIONS OF GIANT STARS

2.1. The white dwarf fraction

Consider an open star cluster of age τ . The cluster’s turnoff mass, m_τ , defines the threshold above which stars have evolved off the main sequence. Now, suppose a binary system is identified in this cluster, where the primary star is a red giant of mass m_{RG} , and the secondary is too faint to be directly identified. The mass of the secondary can be constrained indirectly from the orbital motion of the primary. However, determining its

exact nature based solely on the orbital elements and primary mass is challenging. For example, without additional information, it is difficult to determine whether a $\sim 0.6 M_\odot$ companion of a red giant is a white dwarf or a late-type main sequence star (e.g., Shahaf et al. 2019). Nevertheless, compared to unequivocal classification, statistical estimates are often more feasible.

The occurrence rate of white dwarf companions stems from the properties of the primordial, zero-age main sequence population. To model it, assume that the distribution of primordial primary masses, m_1 , is similar to the Salpeter (1955) initial mass function, where α signifies the exponential index of the distribution. The primordial mass ratio distribution is taken to be flat so that the secondary mass, m_2 , is uniformly distributed between 0 and m_1 . These assumptions yield a bivariate density function,

$$\Phi(m_1, m_2) \propto m_1^{-(\alpha+1)} \quad (1)$$

if $0 < m_2 \leq m_1$ and zero otherwise. The impact of deviations from uniformity on the inferred properties of the sample is discussed below.

To assess the probability of the secondary companion being a white dwarf, we consider two possible scenarios: first, that the present-day giant star is also the primordial primary, and second, that it is the primordial secondary. In the first scenario, m_1 can be identified with m_{RG} , assuming insignificant mass loss. Equation (1) suggests the fraction of systems in this state, P_{MS} , is proportional to $m_{\text{RG}}^{-\alpha}$. In this case, the secondary companion is most likely a main-sequence star. Other, less common, evolutionary scenarios are also possible but presumably occur much less frequently.

In the second scenario, the faint star was originally more massive and has already evolved into a compact object. Most likely a white dwarf. This requires the primordial primary to have been massive enough to complete its post-main-sequence evolution, i.e., $m_1 > m_\tau + \Delta$, where Δ is the gap between the turn-off mass and the least massive white dwarf progenitor star. Since the red giant was originally the primordial secondary, $m_{\text{RG}} \simeq m_2$. This primordial secondary is now a red giant, therefore, we can place bounds on its mass: $m_\tau < m_2 < m_\tau + \Delta$. From equation (1), the fraction of systems with white dwarf companions, P_{WD} , is approximately proportional to $\alpha^{-1}(m_\tau + \Delta)^{-\alpha}$.

The odds ratio between the two cases does not depend on the proportion coefficients,

$$O_{\text{WD}} \equiv \frac{P_{\text{WD}}}{P_{\text{MS}}} \simeq \frac{1}{\alpha} \left(\frac{m_{\text{RG}}}{m_\tau} \right)^\alpha \left(1 + \frac{\Delta}{m_\tau} \right)^{-\alpha}. \quad (2)$$

In the following, it is assumed that the contribution of other configurations, such as stripped stars, triple systems, or neutron stars, is small. Hence, $P_{\text{WD}} + P_{\text{MS}} \simeq 1$ and the fraction of white dwarf companions is

$$P_{\text{WD}} \simeq \frac{O_{\text{WD}}}{1 + O_{\text{WD}}}. \quad (3)$$

Next, we use this expression to describe the mass ratio distribution of the sample.

2.2. The mass ratio distribution

The mass ratio of a binary system, q , is defined as the mass of the faint secondary component, whether a main-sequence star (m_{MS}) or a white dwarf (m_{WD}), divided by the mass of the luminous red giant primary, m_{RG} .

The sample's mass ratio distribution consists of two components: one for the sub-population in which the red giant is the primordial primary and another where it is the primordial secondary. In the first case, assuming negligible mass loss or transfer during the giant's evolution, the mass ratio distribution should remain flat. Alternatively, if the red giant was the primordial secondary, the white dwarf progenitor lost a substantial fraction of its mass, changing the distribution's shape. Therefore, the resulting mass ratio distribution can be expressed as

$$f_q = (1 - P_{\text{WD}}) + P_{\text{WD}} \cdot f_q^{\text{WD}}. \quad (4)$$

The first term represents the uniformly distributed systems from the first scenario, and the second term represents systems where the companion has evolved into a white dwarf. To fully describe the mass ratio distribution, it is necessary to define f_q^{WD} .

The white dwarf progenitor is initially the primordial primary star, with a mass denoted as m_{PR} (equivalent to m_1). Consequently, the white dwarf mass distribution follows a truncated power law with the same exponential index as the mass distribution from equation (1), namely, it is proportional to $m_{\text{PR}}^{-(\alpha+1)}$. This power-law distribution is truncated by the Chandrasekhar limit from above and by the remnant mass of the least massive progenitor (approximately $m_\tau + \Delta$; see above) from below. The progenitor's mass relates to that of the white dwarf through the IFMR, which, for simplicity, is modeled as a linear relation,

$$m_{\text{WD}} = A m_{\text{PR}} + B. \quad (5)$$

Using the inverse relation, it follows that the m_{WD} distribution is proportional to $(m_{\text{WD}} - B)^{-(\alpha+1)}$.

Consider the mass ratio distribution of a binary system with a red giant of some fixed mass, m_{RG} . In this

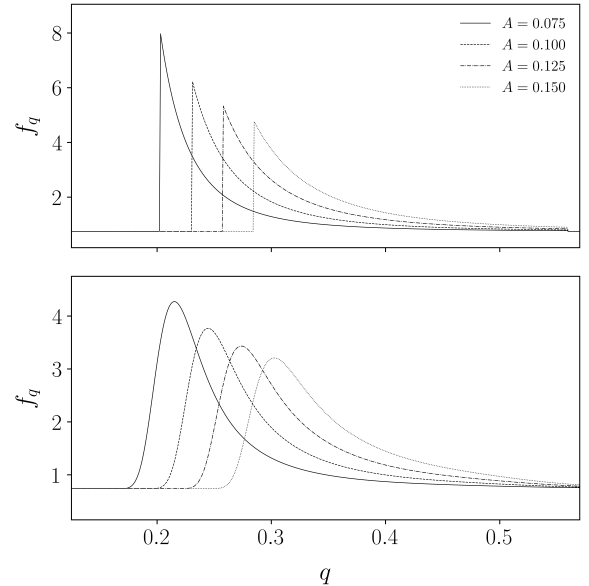


Figure 1. *Top panel* – The mass ratio distribution from equation (4), for several IFMR slopes (see legend) and a fixed intercept (B) of $0.3 M_\odot$. The distributions were calculated assuming a red giant mass of $2.50 M_\odot$, turnoff mass of $2.25 M_\odot$, and $\Delta = 0.5 M_\odot$. The initial mass function exponent used is $\alpha = 2.35$. *Bottom panel* – the corresponding marginal mass ratio distribution derived assuming the uncertainty in the giant's mass is $0.25 M_\odot$, and $m_\tau = m_{\text{RG}} - \Delta/2$. Line styles represent the same parameters as in the top panel.

case, the mass ratio distribution inherits the truncated power-law form. Probability density functions of this type are often referred to as *generalized Pareto distributions*. The distribution is characterized by the initial mass function exponent, α , and three additional parameters: q_{B} , q_{L} , and q_{H} . The resulting distribution is

$$f_q^{\text{WD}} = \zeta_0 (q - q_{\text{B}})^{-(\alpha+1)} \quad (6)$$

if $q \in (q_{\text{L}}, q_{\text{H}})$ and zero otherwise. The mass-ratio parameters satisfy $q_{\text{B}} < q_{\text{L}} < q_{\text{H}}$, and ζ_0 is a normalization constant, where

$$\zeta_0 = \alpha \frac{(q_{\text{H}} - q_{\text{B}})^\alpha (q_{\text{L}} - q_{\text{B}})^\alpha}{(q_{\text{H}} - q_{\text{B}})^\alpha - (q_{\text{L}} - q_{\text{B}})^\alpha}.$$

Notably, the mass of the giant and evolutionary phase do not appear explicitly in equation (6). Therefore, the requirement that the primary star is a red giant can be relaxed. This will be discussed later when prospective samples are considered for analysis.

The distribution parameters are related to the IFMR from equation (5) through the following relations:

$$\begin{aligned} q_{\text{B}} &\simeq B/m_{\text{RG}}, \\ q_{\text{L}} &\simeq A(m_\tau + \Delta)/m_{\text{RG}} + q_{\text{B}}, \quad \text{and} \\ q_{\text{H}} &\simeq 1.4 M_\odot/m_{\text{RG}}. \end{aligned} \quad (7)$$

The top panel of Figure 1 illustrates the shape of the obtained mass ratio distribution. In practice, the giant’s mass, m_{RG} , is estimated up to some uncertainty, δm . This uncertainty should soften the sharp features of the distribution, as it affects the cut-off values from equation (7). Therefore, averaging out the giant’s mass could provide a more realistic distribution visualization. This approach is demonstrated in the bottom panel of Figure 1, where the giant’s mass is assumed to be normally distributed.

The peak of the distribution originates from the lower cut-off mass ratio, q_L . While marginalizing over the giant’s mass smooths the distribution, the peak remains a prominent and localized feature. Since q_L is sensitive to the parameters of the IFMR, so is the position of the peak, q_p . Therefore, it could provide immediate insights upon inspection. As a crude approximation, we take

$$q_p \approx A(1 + \varepsilon) + q_B, \quad (8)$$

where ε is on the order of 10^{-1} , and the approximation accuracy degrades roughly like $(\delta m/m)^2$. Figure 2 illustrates the peak’s position as a function of the slope and intercept of the IFMR.

2.3. The modified mass function distribution

Empirical studies of spectroscopic binaries can, in principle, constrain the white dwarf IFMR across a wide range of orbital separations and evolutionary scenarios. However, the red giant dominates the system’s emitted flux in most cases. Thus, only the spectral lines originating from the giant are detected, and only the giant’s velocities are measured. As a result, the mass ratio, q , and orbital inclination, i , cannot be independently derived.

However, if sufficient radial velocity measurements are obtained, the orbital period, radial velocity semi-amplitude, and eccentricity can be fitted to reproduce the observed orbital modulation. The mass function, f_m , can be derived from these orbital parameters. The ratio between f_m and m_{RG} often called the reduced mass function, can be expressed as a combination of the mass ratio and orbital inclination:

$$y \equiv \frac{f_m}{m_{\text{RG}}} = \frac{q^3}{(1+q)^2} \sin^3 i. \quad (9)$$

Notably, each value of y is associated with a minimal possible mass ratio, Q_y , which is determined by setting the inclination to 90° .

The reduced mass function distribution is obtained by assuming that the binary’s orbital plane is randomly oriented. However, deriving the underlying mass ratio distribution from an observed set of reduced mass function

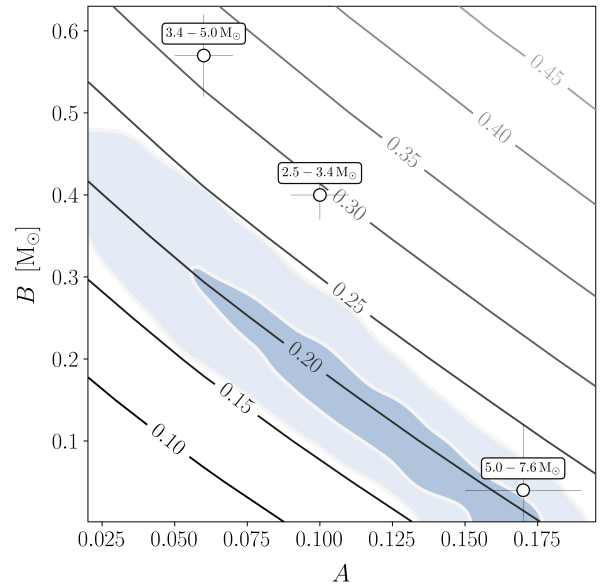


Figure 2. The position of the peak of the mass ratio distribution, as a function of the IFMR slope (A) and intercept (B). The solid annotated lines depict the mass-ratio value at which the distribution attains its maximum. The distributions were calculated assuming $m_{\text{RG}} = 2.4 \pm 0.4 M_\odot$, $\Delta = 0.5 M_\odot$, $\alpha = 2.35$. The open circles represent the IFMR parameters fitted by Cunningham et al. (2024). The light-blue shading represents the 1 and 2σ levels of the derived IFMR (see Section 3).

values is not straightforward (e.g., Mazeh & Goldberg 1992; Boffin et al. 1993; Heacox 1995). To address this challenge, Shahaf et al. (2017) introduced the *modified mass function*,

$$S \equiv 1 - \int_{Q_y}^1 \sqrt{1 - y^{2/3} (1+q)^{4/3} q^{-2}} dq. \quad (10)$$

Unlike the reduced mass function, the modified mass function distribution, f_S , qualitatively follows the shape of the underlying mass ratio distribution. The expression to derive f_S from f_q is available in Appendix A.

The similarity between f_S and f_q can be used to constrain the IFMR. The top panel of Figure 3 presents the resulting distribution of the modified mass function for the same set of parameters used in Figure 1. The relationship between the peak positions of the two distributions may be useful. The relation between the peak positions of f_S and f_q for the parameter space considered in Figure 2 roughly follows the relation

$$\log_{10} q_p \simeq 0.20 \log_{10}^2 S_p + 1.30 \log_{10} S_p - 0.08, \quad (11)$$

where q_p and S_p are the values at which the mass ratio and modified mass function distributions attain their maximum.

2.4. A Synthetic population

We constructed a synthetic sample of binary stars to evaluate an approximated analytical expression for the mass ratio and the modified mass function distribution. This sample was generated using the `cogsworth`¹ package (Wagg et al. 2024), which integrates with the COSMIC population synthesis code (Breivik et al. 2020).

The synthetic population parameters were set to produce a simplistic scenario and aim to avoid common envelope evolution, significant mass transfer phases, or strong tidal interactions. The fiducial binary orbits were assumed circular, with periods uniformly distributed between 100 and 200 years. Primordial primary masses followed the Salpeter (1955) initial mass function, while secondaries were drawn from a flat mass ratio distribution. A fixed metallicity of 0.2 dex was applied across the population, and the white dwarf IFMR was modeled using the Han et al. (1995) relation.

The synthetic population evolved over 1 Gyr. To isolate binaries containing a red giant, we selected systems with a COSMIC `kstar` index of 2, 3, or 4, corresponding to stars on the Hertzsprung gap, first giant branch, or helium-burning phase. We restricted the companions of these red giants to main-sequence stars (`kstar` 0 or 1), white dwarfs (`kstar` 10, 11, or 12), or additional red giants of lower mass. To minimize the effects of binary interaction, evolved systems with orbital periods under 10 years were excluded. The simulation and these criteria yielded a synthetic sample of $\sim 14,000$ binaries.

Figure 4 presents histograms of the mass ratio and the modified mass function for the synthetic sample. The histograms distinguish subpopulations of giants paired with main-sequence stars, white dwarfs, or other giants. Most systems with main-sequence companions appear in light gray, while systems with white dwarf companions are shown as white bars. At near-unity mass ratios, the population predominantly comprises pairs of giant stars. The truncation at mass ratios below 0.1 arises from the absence of sub-stellar companions in the simulation.

The expected f_q and f_s distributions are overlaid on the histograms in Figure 4. The red giant masses in the synthetic sample are not normally distributed. However, to align with prior discussions and figures, we assumed m_{RG} is Gaussian and used the mean and standard deviation of the red giants in the synthetic sample (2.25 and 0.05 M_{\odot} , respectively). The initial mass function exponent was set to the Salpeter value of 2.35, and Δ was set to 0.25 M_{\odot} . We inspected 0.8–1 Gyr Solar-

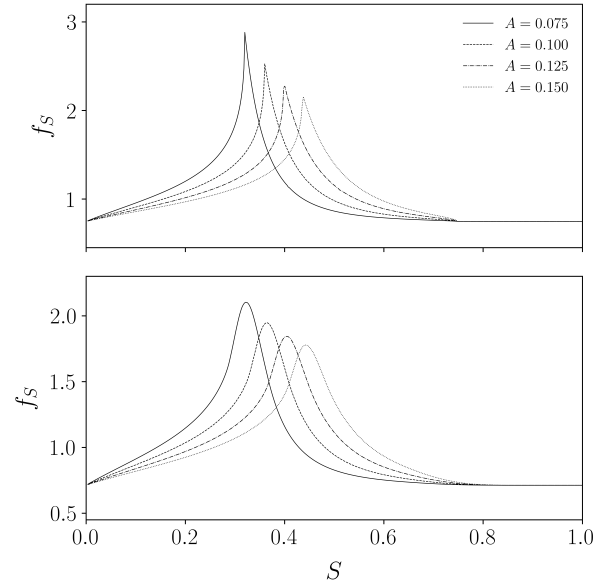


Figure 3. The modified mass function distributions for red giants in open clusters. The top and bottom panels plots were produced using the same parameters as in Figure 1.

metallicity PARSEC² isochrones to justify the latter selection (Bressan et al. 2012; Chen et al. 2014, 2015; Tang et al. 2014). Finally, we adopted an IFMR of

$$m_{\text{WD}} = 0.104 m_{\text{PR}} + 0.36 M_{\odot}.$$

This relation corresponds to one segment of the broken linear relation proposed by Han et al. (1995), which best fits the distribution. The figure shows that the analytical prescription describes the synthetic distribution even without a detailed fitting procedure. This example shows how the equation (4) can describe the distribution if the IFMR is known. In Section 3, we consider the inverse problem of inferring the IFMR from a set of observed binary orbits.

2.5. Detection function

The discussion above assumes an idealized scenario where all target population binaries are equally detectable, which is false in actual samples. However, a detection bias arising from finite instrumental precision can limit the detectability of systems with low mass ratios. Here, we consider a detection function, \mathcal{D} , for a sample of spectroscopic binaries, following the method of Mazeh & Goldberg (1992).

The detection function is estimated by assuming that the survey is characterized by a radial velocity semi-

¹ Available online at cogsworth.readthedocs.io.

² PAdova and tRieste Stellar Evolution Code, version 1.2S, available online via stev.oapd.inaf.it/cmd.

amplitude threshold, K_{th} , below which binaries remain undetected. The orbital speed of a binary in a circular orbit is determined by its mass ratio, q , orbital period, P , and primary mass, m_{RG} . The detectability of a system is reduced to the span of orbital inclinations in which the radial component of the orbital speed exceeds the detection threshold. The critical inclination, i_c , below which detection is impossible, is given by

$$\sin i_c = K_{\text{th}} \left(\frac{1}{2\pi G} \frac{P}{m_{\text{RG}}} \right)^{1/3} \frac{(1+q)^{2/3}}{q}. \quad (12)$$

The detection function quantifies the detection probability. Assuming that the orbits are randomly oriented,

$$\mathcal{D}(q) = \sqrt{1 - \sin^2 i_c}. \quad (13)$$

See [Mazeh & Goldberg \(1992\)](#) for a detailed derivation of this relation. Examples can be found also in [Shahaf et al. \(2017\)](#) and [Shahaf & Mazeh \(2019\)](#).

The resulting correction function is a multiplicative factor imposed on the mass ratio distribution. The model for the observed biased distribution is, therefore, given by replacing the idealized model for f_q from Equation (4) with the corrected version, namely

$$f_q^{\text{obs}} \propto f_q \times \mathcal{D}. \quad (14)$$

This probability density function inherits the parameters of equations and (4), (6), and (13). Since f_q is normalized, the normalization constant depends on the parameters of the detection function.

3. A TEST CASE: THE MERMILLIOD SAMPLE

3.1. Sample description

In an extensive spectroscopic campaign spanning ~ 20 years, [Mermilliod et al. \(2007b\)](#) monitored 1309 red giants across 187 open clusters, achieving a typical radial velocity accuracy of $\sim 0.4 \text{ km s}^{-1}$. They identified 289 spectroscopic binaries and provided orbital solutions for 156 of these systems. [North \(2014\)](#) estimated the mass ratio distribution of the binaries in this sample and identified a peak corresponding to secondaries of $\sim 0.6 M_{\odot}$ and suggested it stems from a population of white dwarf companions. North also noted that their mass distribution seemed inconsistent with the expected IFMR.

In a subsequent study, [Van der Swaelmen et al. \(2017\)](#) validated the cluster membership of the binaries in this sample. After filtering out systems with low cluster membership probability, they provided reliable mass estimates for 125 red giants and derived the mass ratio distribution of the sample. Their finding corroborated

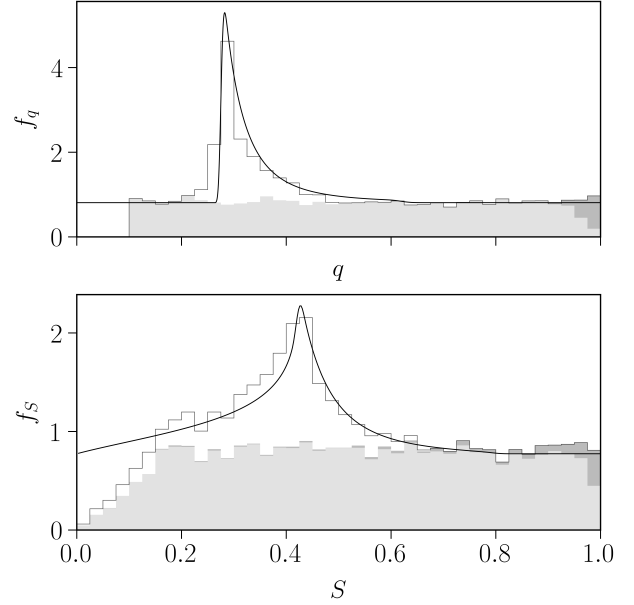


Figure 4. Mass ratio (top panel) and modified mass function (bottom panel) distribution of the synthetic population generated by `cogsworth`. The color of the histogram bin indicates the type of secondary companion: white, light gray, and dark gray bins represent white dwarfs, main sequence, and evolved giant secondaries, respectively. The thin black lines represent the expected shape of the distribution according to the analytical prescription (see text).

the results of [North \(2014\)](#). The full list, including mass estimates, is available online (see table A.4 therein). We select a subsample of 69 systems with red giant primaries less massive than $3.25 M_{\odot}$ and orbital periods between 0.5 and 20 years. Figure 5 shows histograms of red giant mass, radial velocity semi-amplitude, logarithm of orbital period, and orbital eccentricity.

The binaries in the selected sample are associated with 21 different open clusters, listed in a supplementary table. The clusters have ages around $0.83_{-0.24}^{+0.73}$ Gyr and near-solar metallicities of $[\text{Fe}/\text{H}] \simeq 0.0_{-0.1}^{+0.2}$ dex ([Dias et al. 2021](#); [Hunt & Reffert 2023](#)). Two systems have minimum mass ratios above one: star 4 in NGC 1528 and star 70 in NGC 6633, with \mathcal{Q}_y of 1.10 ± 0.05 and 1.07 ± 0.02 , respectively. As demonstrated above, some binaries with mass ratios close to unity are expected to comprise two evolved stars. These systems are, therefore, retained and treated as equal mass binaries (modified mass function set to one).

Figure 6 shows a histogram of the sample’s modified mass function values. Using the rightmost histogram bins, we estimate $P_{\text{WD}} \approx 0.25$ and estimate that the peak of the distribution is positioned at $S_p \approx 0.29$. Equation (11) identifies this peak with $q_p \approx 0.185$, suggesting

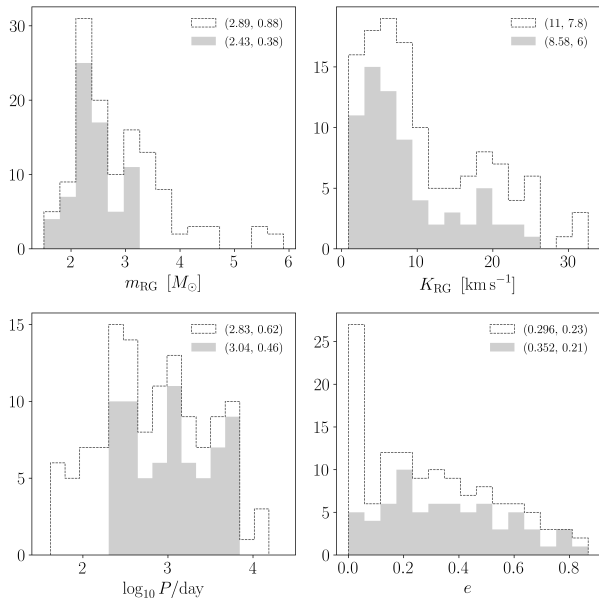


Figure 5. The properties of the sample. Clockwise from the top-left panel: histograms of the red giant mass, radial velocity semi amplitude, orbital eccentricity, and logarithm of the orbital period. The grey bars show the distribution selected subsample of 69 systems and the entire sample of 125 binaries is overlaid as a black dashed line. The legends of each panel provide the mean and standard deviation of each quantity.

that $A \sim 0.2$, assuming the intercept value is negligible. With these preliminary estimates, we now infer the distribution’s parameters.

3.2. Inference

For brevity, use θ to represent the parameters of the distribution (P_{WD} , q_B , q_L , q_H , α , and K_{th}). In addition, the distribution depends on each binary’s primary mass and orbital period through the detection function. To simplify the inference, these values are fixed at nominal literature values. The likelihood of the i^{th} spectroscopic binary is given by

$$\mathcal{L}_i(\theta | S_i) = f_S^{\text{obs}}(S_i | \theta, m_{\text{RG},i}, P_i). \quad (15)$$

The term on the right-hand side represents the modified mass function distribution corresponding to the mass ratio distribution from equation (14), derived according to the prescription in Appendix A. The equation above does not account for the measurement uncertainty in the modified mass function. While this compromise may be

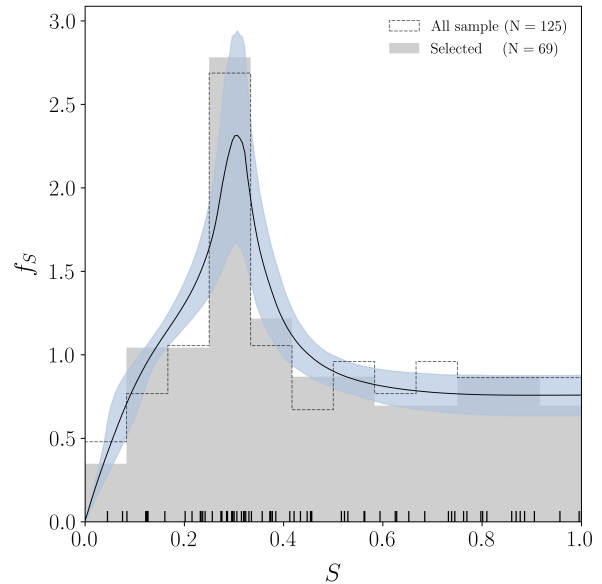


Figure 6. A histogram showing the modified mass function values of the sample. Grey bars show the distribution selected subsample of 69 systems and the entire sample of 125 binaries is overlaid as a black dashed line. The black ticks at the bottom of the figure indicate the position of individual targets in the selected samples. The solid black line shows the expected shape of the distribution, using the fitted parameters from Section 3 and after accounting for the radial velocity detection threshold, \mathcal{D} . The light blue area represents the corresponding one-sigma confidence interval.

acceptable in some cases, a more general consideration may be required.³

The parameters are determined by sampling the logarithm of the posterior distribution:

$$\log P(\theta | \{S_i\}) = \sum_i \log \mathcal{L}_i(\theta | S_i) + \log \pi(\theta), \quad (16)$$

where π represents the prior distribution of the fitted parameters. A normal prior is applied to q_H (mean 0.58, standard deviation 0.10), while flat priors are used for P_{WD} , q_B , and q_L within $0 < P_{\text{WD}} < 1$ and $0 < q_B < q_L < q_H < 1$. The prior for K_{th} is flat between 0 and 5 km s^{-1} , and α is assumed to be normally distributed around 2.35, with a standard deviation of 0.30.

The analysis is performed on the 69 selected systems described above. To estimate the parameters, we used **emcee** (Foreman-Mackey et al. 2013), with 50 walkers taking 5000 steps each. Figures 6 and 7 show the esti-

³ The reduced mass function (y) is a ratio of two quantities. Assuming measurement errors are Gaussian distributed, the normal ratio distribution (e.g., Hinkley 1969) can provide the uncertainty estimates for y , which can be incorporated into the likelihood.

estimated f_S distribution and posterior corner plots. Evidently, the analysis provides tighter constraints on q_L than on q_B , as expected for heavy-tailed distributions. Cutoff values, such as q_L , are frequently sampled, while tail values, determining q_B , are rare. Consequently, q_B is constrained to an upper limit of ~ 0.2 , with values below ~ 0.15 being roughly equally probable. The estimated parameter values, based on the 16th, 50th, and 84th posterior percentiles, are:

$$\begin{aligned} P_{\text{WD}} &= 0.29^{+0.10}_{-0.11}, & q_B &= 0.088^{+0.064}_{-0.057}, \\ q_L &= 0.189^{+0.017}_{-0.015}, & q_H &= 0.58^{+0.10}_{-0.10}. \end{aligned} \quad (17)$$

The estimated detection threshold for radial velocity, K_{th} , is $1.1 \pm 0.5 \text{ km s}^{-1}$. The sample does not constrain the initial mass function, yielding $\alpha = 2.36 \pm 0.29$.

Using posterior samples of the mass ratio distribution, we estimated the white dwarf mass distribution in our sample through a Monte Carlo experiment. For each posterior step in the `emcee` chain, a primary mass was randomly assigned, assuming $m_{\text{RG}}/M_{\odot} \sim \mathcal{N}(2.4, 0.4^2)$. The white dwarf mass distribution was computed on a predefined mass grid based on the posterior samples, the assigned giant mass, and equation (7). Repeating this procedure generated an ensemble of m_{WD} distributions. The distribution shown in Figure 8 was obtained by averaging the values at each grid point. The blue-shaded region spans the 16th to 84th percentiles ($0.43\text{--}0.73 M_{\odot}$). Vertical lines indicate the distribution’s mode, median, and mean ($0.50, 0.54, \text{ and } 0.58 M_{\odot}$, respectively). The mean mass estimate is consistent with the results reported by North (2014) and Van der Swaelmen et al. (2017). However, the analysis relies on the heavy-tailed Pareto distribution, suggesting that most white dwarfs are less massive than this mean value. Interestingly, the white dwarfs in this sample are less massive than expected, given their expected progenitor masses. This is discussed further below.

Now, we use the fitted parameters of the distribution to constrain the IFMR: the parameters of equation (5) were derived from the posterior samples, assuming the red giant’s current mass closely approximates its zero-age main-sequence mass. For each posterior sample, a primary mass was drawn as described earlier, and a random mass gap was assigned, where $\Delta/M_{\odot} \sim \text{Uniform}(0.2, 0.4)$; see the discussion in Section 2.4. The turn-off mass was then calculated using equation (2), with samples retained only if $m_{\tau} < m_{\text{RG}} < m_{\tau} + \Delta$. The IFMR slope and intercept were determined using equations (5) and (7). Repeating this process yielded a distribution of IFMR parameters.

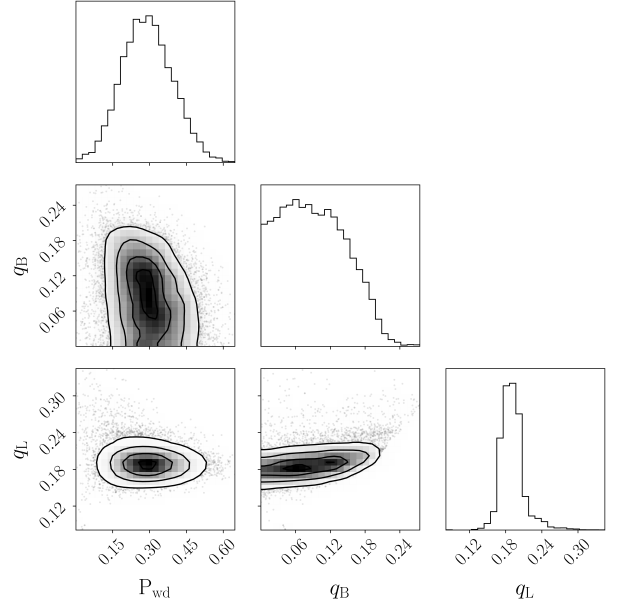


Figure 7. A corner plot depicting the posterior distribution of the first three fitted parameters. The white dwarf fraction, P_{WD} , and mass ratio cutoff value, q_L , are well constrained and consistent with the initial qualitative estimates. However, the data is more limited in constraining q_B and sets a firm upper limit at ~ 0.2 , with all values below ~ 0.15 equally probable. Two parameters were excluded from the plot, q_H and K_{th} . The full corner plot is available in the online supplementary material.

Considering the sample size and the estimated value of P_{WD} , we expect to have 20 ± 8 white dwarfs in the observed population. This small sample and the strong correlations between the parameters limit the precision of the inferred IFMR. The derived relation is

$$m_{\text{WD}} \simeq (0.097 \pm 0.050) m_{\text{PR}} + (0.19 \pm 0.15) M_{\odot}, \quad (18)$$

where the parameters exhibit a strong linear dependence with a correlation coefficient of -0.89 . Despite these limitations, valuable insights can still be obtained. Figure 2 provides a contour map of the IFMR parameters, showing 1–2 σ confidence levels.

The derived distribution of the parameters aligns with the relation reported by Cunningham et al. (2024) for progenitors more massive than $\sim 5 M_{\odot}$, which is close to a scaling relation. Therefore, to get a better qualitative estimate of the relation, we estimate the IFMR for our sample again using only samples of negligible intercept ($q_B < 1\%$), yielding

$$A_0 \equiv \frac{m_{\text{WD}}}{m_{\text{PR}}} \approx 17.0 \pm 1.3\%. \quad (19)$$

This approximated relation is further discussed below.

4. DISCUSSION

4.1. Evidence for enhanced mass loss

The cutoff value at $q_L \simeq 19\%$ indicates that half of the white dwarfs in this sample have masses below $\sim 0.55 M_\odot$, based on the median value of the corresponding Pareto distribution. The mass distribution in Figure 8 supports this estimate. This result suggests that the white dwarfs in this sample are generally less massive than their field counterparts, which are sharply centered around $0.6 M_\odot$, with only $\sim 10\%$ having masses below $\sim 0.55 M_\odot$ (e.g., Kilic et al. 2020; Jiménez-Esteban et al. 2023; O’Brien et al. 2024).

The discrepancy is more pronounced given that the progenitors in this sample likely exceeded $\sim 2.5 M_\odot$. Current relations predict such progenitors would produce remnants more massive than $\sim 0.65 M_\odot$ (e.g., Cummings et al. 2016; El-Badry et al. 2018; Cunningham et al. 2024; Hollands et al. 2024, but see Andrews et al. 2015; Choi et al. 2016). These white dwarfs are, therefore, 10 – 20% less massive than expected from single-star evolution. A caveat of this argument is the possibility of a significant mass transfer phase, implying that the giants – and consequently the white dwarf progenitors – could have initially been less massive. However, the cluster’s age estimate of ~ 1 Gyr mitigates this concern: with turn-off masses near $2 M_\odot$ (Van der Saelmen et al. 2017), the mass discrepancy remains.

The low masses of these white dwarfs likely reflect the impact of binary interactions. For instance, extremely low-mass white dwarfs ($\lesssim 0.3 M_\odot$) are commonly found in close binary systems with orbital periods of hours to days (Li et al. 2019; Brown et al. 2010, e.g.,). This highlights how binarity can significantly alter stellar evolution, leading to remnants with lower masses. In comparison, the binaries in Mermilliod et al. (2007a) host more massive white dwarfs in systems with significantly wider separations. Thus, the systems in this study likely experienced milder, but still non-negligible, interaction.

With turnoff masses of 2–2.5 M_\odot and using the Salpeter (1955) initial mass function, the median progenitor mass for the white dwarfs in this sample is estimated to be 3–3.5 M_\odot . This narrow range justifies applying the scaling relation in equation (19) instead of the linear model in equation (18). The scaling relation indicates that a typical progenitor in this sample lost 80–85% of its mass while evolving into a white dwarf. While this level of mass loss is consistent with expectations for stars more massive than $\sim 5 M_\odot$ (Cummings et al. 2018), the initial mass function suggests that at least 80% of the progenitors had initial masses below $\sim 5 M_\odot$, where the expected mass loss fraction is closer

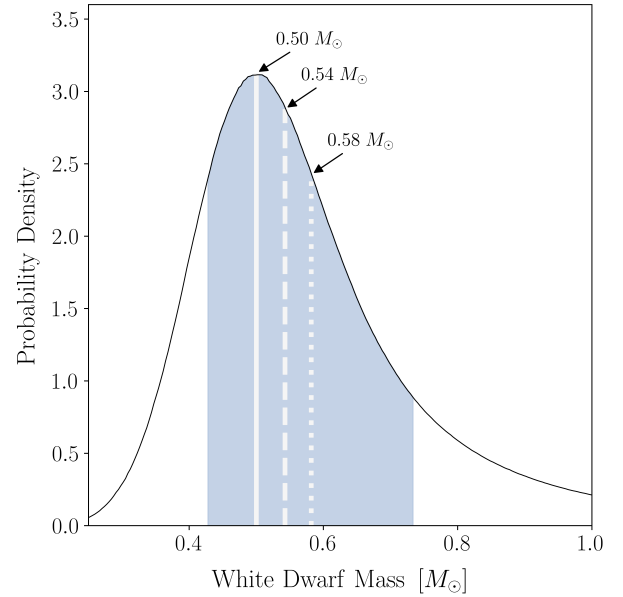


Figure 8. The derived white dwarf mass distribution, based on analyzing the selected sample of 69 binary systems, out of which 20 ± 8 systems comprise a red giant with a white dwarf companion. The solid black line depicts the estimated mass probability density function. The blue-shaded area covers the 16th to 84th percentile range ($0.43 - 0.73 M_\odot$). The solid, dashed, and dotted white lines illustrate the position of the distribution’s mode, median, and mean.

to 75%. This implies an additional $\sim 0.2 M_\odot$ of mass loss, likely due to binary interactions.

Still, while this analysis estimates the amount of mass loss, it does not determine how or during which evolutionary phase the mass was lost. Nonetheless, despite the modest sample size, the analysis effectively constrains the properties of the population.

4.2. Assumptions and limitations

The analysis above relies on several assumptions. First, the primordial mass ratio distribution is assumed to be flat. Admittedly, this may be an oversimplification, as evidenced by conflicting results in the literature. While some studies suggest that the mass ratio distribution of spectroscopic binaries is indeed flat (Mazeh et al. 2003; Raghavan et al. 2010), others report power-law behavior or a significant population of twin binaries (e.g., El-Badry et al. 2019).

The impact of a population of twins is relatively straightforward to address. Equal-mass binaries leave the main sequence roughly simultaneously, making it possible to identify both components in some cases. Moreover, twins produce a distinct peak in the mass ratio distribution, which is well-separated from the white

dwarf Pareto peak for giants more massive than $\sim 1 M_{\odot}$. This separation enables their inclusion in the analysis by explicitly accounting for their contribution or parameterizing it as needed. A non-uniform mass ratio distribution poses a more significant challenge, as it affects both the estimated fraction of white dwarfs and the shape of their mass distribution. Nevertheless, assuming a flat distribution provides a reasonable first approximation, given the current sample size. Most conclusions in this work rely on the position of the distribution’s peak, corresponding to the least massive progenitor capable of evolving into a white dwarf. This key property is robust against variations in the underlying mass ratio distribution. The model can be generalized further to account for non-uniform distribution if needed.

The assumed shape of the initial mass function may also influence the results. This consideration is particularly relevant given the possibility that it is not universal. The exponent, α , affects the white dwarf fraction and the slope of the mass distribution but not its cutoff value. The prior used in this analysis is consistent within roughly 1σ with the initial mass function exponent found for the thin disk, thick disk, and high-metallicity halo by Hallakoun & Maoz (2021, $2.05 \lesssim \alpha \lesssim 2.75$). However, the sample analyzed in this work is not large enough to constrain α . Nevertheless, when considering larger samples or populations obtained from distinct Galactic environments, the assumptions regarding the initial mass function could become more significant.

Another limitation of the method presented here stems from the inherent covariance between the parameters of the IFMR. These parameters are related to one another through the mass ratio cutoff value, q_L , as equation (7) shows. Strong constraints on q_B are required to mitigate this degeneracy, but these are difficult to achieve with small sample sizes, as they depend on accurate estimates of the distribution slope. Nevertheless, by leveraging simple supporting arguments, the analysis above offers meaningful insights into the history of mass loss in these systems.

5. SUMMARY AND CONCLUSIONS

This study demonstrates the utility of mass ratio distributions as a tool to probe the influence of binarity on stellar evolution. The truncated Pareto profile used to describe the population provides effective constraints on the properties of white dwarfs and their progenitors. Analysis of the Mermilliod et al. (2007b) sample reveals that, in the explored regime of orbital separations, white dwarfs are $\sim 20\%$ less massive than their isolated counterparts. The findings suggest that their progeni-

tors experienced enhanced mass loss of approximately $\sim 0.2 M_{\odot}$ due to binary interactions.

Mass transfer and binary co-evolution in this regime, on the cusp of a common envelope phase, is not fully understood. Investigating the relationship between white dwarf mass and binary system properties will help constrain the dominant mechanisms and quantify their role in shaping the population. Expanding the analysis to larger samples will enable the search for dependence between the white dwarf properties and the system’s physical parameters, such as orbital separation, eccentricity, and chemical composition. Such a dependency, if detected, could yield insights into the final stages of stellar evolution (e.g., Shahaf et al. 2023, 2024; Hallakoun et al. 2024; Yamaguchi et al. 2024b,a).

With larger samples, further work can also focus on stellar core growth during the giant and asymptotic giant branch phases. The *Gaia* third data release has already provided valuable opportunities for this purpose (e.g., using the Hunt & Reffert 2023, catalog). These samples can help constrain the IFMR for binaries with intermediate separations (Ironi et al., in preparation). Moreover, additional observations, such as measurements of Barium enhancement, can reveal whether the white dwarf progenitor underwent an asymptotic giant phase while providing independent constraints on its mass (e.g., Rekhi et al. 2024). Such constraints can, in turn, identify when core growth is interrupted and statistically evaluate its impact on the remnant’s mass. Observations of this kind can probe the mass accumulation rate during the asymptotic giant branch phase (Marigo et al. 2022; Marigo 2022; Addari et al. 2024).

Another promising avenue to increase sample sizes is to relax the requirement for red giants to belong to open clusters. For example, chemical abundance indicators, such as carbon-nitrogen ratios, can help identify suitable red giant systems for study (e.g., Roberts et al. 2024; but see the limitations discussed by Bufanda et al. 2023). Extending the method to binaries with main-sequence companions could also be viable; since the red giant’s evolutionary state does not directly affect the mass ratio distribution, such systems could offer complementary insights. However, potential biases introduced by age heterogeneity in main-sequence systems must be carefully mitigated to ensure reliable results. Data from *Gaia* and next-generation surveys will be instrumental in refining this framework and uncovering new details about the final stages of stellar evolution.

I thank the anonymous referee for the helpful comments and suggestions. I thank Tsevi Mazeh and Simchon Faigler for their contributions during the early stages of this work, and I am grateful to Na’ama Hallakoun for her invaluable advice and support. I also thank Sagi Ben-Ami, Dotan Gazith, Oryna Ivashtenko, Dan Maoz, Eran Ofek, Hans-Walter Rix, Tomer Shenar, and Barak Zackay for their comments and feedback. SS is supported by a Benoziyo Prize Postdoctoral Fellowship. This work is dedicated to the memory of Daniel Alloush and Tom Ish-Shalom; you will not be forgotten.

Software: This work used `cogsworth` and its dependencies (Wagg et al. 2024; Wagg et al. 2025; Breivik et al. 2020); the Unified Cluster Catalogue (Perren et al. 2023); `emcee` (Foreman-Mackey et al. 2013); `numpy` (Oliphant 2006; van der Walt et al. 2011); and `scipy` (Virtanen et al. 2020).

APPENDIX

A. THE REDUCED AND MODIFIED MASS FUNCTIONS DISTRIBUTION

For a given mass ratio distribution, the reduced mass function distribution can be obtained by assuming that the orbital plane of motion is randomly oriented (e.g., Heacox 1995, Shahaf et al. 2017). The distribution is expressed in an integral form,

$$f_y(y; f_q) = \int_{\mathcal{Q}_y}^1 f_q(q) \mathbb{K}[y, q] dq, \quad (\text{A1})$$

where

$$\mathbb{K}(y, q) = \frac{(1+q)^{4/3}}{3 y^{1/3} q \sqrt{q^2 - y^{2/3}(1+q)^{4/3}}}.$$

The modified mass function distribution, f_S , is related to that of the reduced mass function via

$$f_S(S; f_q) = \frac{f_y[y(S); f_q]}{f_y[y(S); 1]} \quad (\text{A2})$$

where $y(S)$ is the inverse function of equation (10). The distribution of S mimics the functional shape of the unknown mass ratio distribution, as demonstrated in Figure 3. For additional examples of using the modified mass function as a proxy for the mass ratio distribution, see Shahaf & Mazeh (2019).

REFERENCES

- Addari, F., Marigo, P., Bressan, A., et al. 2024, *ApJ*, 964, 51, doi: [10.3847/1538-4357/ad2067](https://doi.org/10.3847/1538-4357/ad2067)
- Althaus, L. G., Córscico, A. H., Isern, J., & García-Berro, E. 2010, *A&A Rv*, 18, 471, doi: [10.1007/s00159-010-0033-1](https://doi.org/10.1007/s00159-010-0033-1)
- Andrews, J. J., Agüeros, M. A., Gianninas, A., et al. 2015, *ApJ*, 815, 63, doi: [10.1088/0004-637X/815/1/63](https://doi.org/10.1088/0004-637X/815/1/63)
- Barrientos, M., & Chanamé, J. 2021, *ApJ*, 923, 181, doi: [10.3847/1538-4357/ac2f49](https://doi.org/10.3847/1538-4357/ac2f49)
- Beuther, H., Ahmadi, A., Mottram, J. C., et al. 2019, *A&A*, 621, A122, doi: [10.1051/0004-6361/201834064](https://doi.org/10.1051/0004-6361/201834064)
- Boffin, H. M. J., Cerf, N., & Paulus, G. 1993, *A&A*, 271, 125
- Breivik, K., Coughlin, S., Zevin, M., et al. 2020, *ApJ*, 898, 71, doi: [10.3847/1538-4357/ab9d85](https://doi.org/10.3847/1538-4357/ab9d85)
- Bressan, A., Marigo, P., Girardi, L., et al. 2012, *MNRAS*, 427, 127, doi: [10.1111/j.1365-2966.2012.21948.x](https://doi.org/10.1111/j.1365-2966.2012.21948.x)
- Brown, W. R., Kilic, M., Allende Prieto, C., & Kenyon, S. J. 2010, *ApJ*, 723, 1072, doi: [10.1088/0004-637X/723/2/1072](https://doi.org/10.1088/0004-637X/723/2/1072)
- Bufanda, E., Tayar, J., Huber, D., Hesselquist, S., & Lane, R. R. 2023, *ApJ*, 959, 123, doi: [10.3847/1538-4357/acf9a5](https://doi.org/10.3847/1538-4357/acf9a5)
- Chen, Y., Bressan, A., Girardi, L., et al. 2015, *MNRAS*, 452, 1068, doi: [10.1093/mnras/stv1281](https://doi.org/10.1093/mnras/stv1281)
- Chen, Y., Girardi, L., Bressan, A., et al. 2014, *MNRAS*, 444, 2525, doi: [10.1093/mnras/stu1605](https://doi.org/10.1093/mnras/stu1605)
- Cheng, S., Cummings, J. D., Ménard, B., & Toonen, S. 2020, *ApJ*, 891, 160, doi: [10.3847/1538-4357/ab733c](https://doi.org/10.3847/1538-4357/ab733c)
- Choi, J., Dotter, A., Conroy, C., et al. 2016, *ApJ*, 823, 102, doi: [10.3847/0004-637X/823/2/102](https://doi.org/10.3847/0004-637X/823/2/102)
- Cummings, J. D., Kalirai, J. S., Tremblay, P.-E., & Ramirez-Ruiz, E. 2016, *ApJ*, 818, 84, doi: [10.3847/0004-637X/818/1/84](https://doi.org/10.3847/0004-637X/818/1/84)
- Cummings, J. D., Kalirai, J. S., Tremblay, P. E., Ramirez-Ruiz, E., & Choi, J. 2018, *ApJ*, 866, 21, doi: [10.3847/1538-4357/aadfd6](https://doi.org/10.3847/1538-4357/aadfd6)
- Cunningham, T., Tremblay, P.-E., & W. O’Brien, M. 2024, *MNRAS*, 527, 3602, doi: [10.1093/mnras/stad3275](https://doi.org/10.1093/mnras/stad3275)

- Dias, W. S., Monteiro, H., Moitinho, A., et al. 2021, MNRAS, 504, 356, doi: [10.1093/mnras/stab770](https://doi.org/10.1093/mnras/stab770)
- Duchêne, G., & Kraus, A. 2013, ARA&A, 51, 269, doi: [10.1146/annurev-astro-081710-102602](https://doi.org/10.1146/annurev-astro-081710-102602)
- El-Badry, K. 2024, NewAR, 98, 101694, doi: [10.1016/j.newar.2024.101694](https://doi.org/10.1016/j.newar.2024.101694)
- El-Badry, K., Rix, H.-W., Tian, H., Duchêne, G., & Moe, M. 2019, MNRAS, 489, 5822, doi: [10.1093/mnras/stz2480](https://doi.org/10.1093/mnras/stz2480)
- El-Badry, K., Rix, H.-W., & Weisz, D. R. 2018, ApJL, 860, L17, doi: [10.3847/2041-8213/aaca9c](https://doi.org/10.3847/2041-8213/aaca9c)
- Fleury, L., Caiazzo, I., & Heyl, J. 2022, MNRAS, 511, 5984, doi: [10.1093/mnras/stac458](https://doi.org/10.1093/mnras/stac458)
- Foreman-Mackey, D., Conley, A., Meierjürgen Farr, W., et al. 2013, emcee: The MCMC Hammer, Astrophysics Source Code Library. <http://ascl.net/1303.002>
- Gentile Fusillo, N. P., Tremblay, P. E., Cukanovaite, E., et al. 2021, MNRAS, 508, 3877, doi: [10.1093/mnras/stab2672](https://doi.org/10.1093/mnras/stab2672)
- Hallakoun, N., & Maoz, D. 2021, MNRAS, 507, 398, doi: [10.1093/mnras/stab2145](https://doi.org/10.1093/mnras/stab2145)
- Hallakoun, N., Shahaf, S., Mazeh, T., Toonen, S., & Ben-Ami, S. 2024, ApJL, 970, L11, doi: [10.3847/2041-8213/ad5e63](https://doi.org/10.3847/2041-8213/ad5e63)
- Han, Z., Podsiadlowski, P., & Eggleton, P. P. 1995, MNRAS, 272, 800, doi: [10.1093/mnras/272.4.800](https://doi.org/10.1093/mnras/272.4.800)
- Heacox, W. D. 1995, AJ, 109, 2670, doi: [10.1086/117480](https://doi.org/10.1086/117480)
- Heintz, T. M., Hermes, J. J., El-Badry, K., et al. 2022, ApJ, 934, 148, doi: [10.3847/1538-4357/ac78d9](https://doi.org/10.3847/1538-4357/ac78d9)
- Hinkley, D. V. 1969, Biometrika, 56, 635, doi: [10.1093/biomet/56.3.635](https://doi.org/10.1093/biomet/56.3.635)
- Holberg, J. B., Oswalt, T. D., Sion, E. M., Barstow, M. A., & Burleigh, M. R. 2013, MNRAS, 435, 2077, doi: [10.1093/mnras/stt1433](https://doi.org/10.1093/mnras/stt1433)
- Hollands, M. A., Littlefair, S. P., & Parsons, S. G. 2024, MNRAS, 527, 9061, doi: [10.1093/mnras/stad3729](https://doi.org/10.1093/mnras/stad3729)
- Hunt, E. L., & Reffert, S. 2023, A&A, 673, A114, doi: [10.1051/0004-6361/202346285](https://doi.org/10.1051/0004-6361/202346285)
- Isern, J., Torres, S., & Rebassa-Mansergas, A. 2022, Frontiers in Astronomy and Space Sciences, 9, 6, doi: [10.3389/fspas.2022.815517](https://doi.org/10.3389/fspas.2022.815517)
- Jiménez-Esteban, F. M., Torres, S., Rebassa-Mansergas, A., et al. 2023, MNRAS, 518, 5106, doi: [10.1093/mnras/stac3382](https://doi.org/10.1093/mnras/stac3382)
- Kilic, M., Bergeron, P., Kosakowski, A., et al. 2020, ApJ, 898, 84, doi: [10.3847/1538-4357/ab9b8d](https://doi.org/10.3847/1538-4357/ab9b8d)
- Kilic, M., Moss, A. G., Kosakowski, A., et al. 2023, MNRAS, 518, 2341, doi: [10.1093/mnras/stac3182](https://doi.org/10.1093/mnras/stac3182)
- Kosakowski, A., Brown, W. R., Kilic, M., et al. 2023, ApJ, 950, 141, doi: [10.3847/1538-4357/acd187](https://doi.org/10.3847/1538-4357/acd187)
- Kuiper, G. P. 1935, PASP, 47, 15, doi: [10.1086/124531](https://doi.org/10.1086/124531)
- Larson, R. B. 1972, MNRAS, 156, 437, doi: [10.1093/mnras/156.4.437](https://doi.org/10.1093/mnras/156.4.437)
- Li, Z., Chen, X., Chen, H.-L., & Han, Z. 2019, ApJ, 871, 148, doi: [10.3847/1538-4357/aaf9a1](https://doi.org/10.3847/1538-4357/aaf9a1)
- Marigo, P. 2022, Universe, 8, 243, doi: [10.3390/universe8040243](https://doi.org/10.3390/universe8040243)
- Marigo, P., Bossini, D., Trabucchi, M., et al. 2022, ApJS, 258, 43, doi: [10.3847/1538-4365/ac374a](https://doi.org/10.3847/1538-4365/ac374a)
- Mazeh, T., & Goldberg, D. 1992, ApJ, 394, 592, doi: [10.1086/171611](https://doi.org/10.1086/171611)
- Mazeh, T., Simon, M., Prato, L., Markus, B., & Zucker, S. 2003, ApJ, 599, 1344, doi: [10.1086/379346](https://doi.org/10.1086/379346)
- Mermilliod, J. C., Andersen, J., Latham, D., & Mayor, M. 2007a, VizieR Online Data Catalog: Orbital elements of 156 spectroscopic binaries (Mermilliod+, 2007), VizieR On-line Data Catalog: J/A+A/473/829. Originally published in: 2007A&A...473..829M, doi: [10.26093/cds/vizieer.34730829](https://doi.org/10.26093/cds/vizieer.34730829)
- Mermilliod, J.-C., Andersen, J., Latham, D. W., & Mayor, M. 2007b, A&A, 473, 829, doi: [10.1051/0004-6361:20078007](https://doi.org/10.1051/0004-6361:20078007)
- Moss, A., Kilic, M., Bergeron, P., Fergard, M., & Brown, W. 2023, MNRAS, 523, 5598, doi: [10.1093/mnras/stad1835](https://doi.org/10.1093/mnras/stad1835)
- North, P. 2014, in Putting A Stars into Context: Evolution, Environment, and Related Stars, ed. G. Mathys, E. R. Griffin, O. Kochukhov, R. Monier, & G. M. Wahlgren, 63–71. <https://arxiv.org/abs/1309.7636>
- O’Brien, M. W., Tremblay, P. E., Klein, B. L., et al. 2024, MNRAS, 527, 8687, doi: [10.1093/mnras/stad3773](https://doi.org/10.1093/mnras/stad3773)
- Offner, S. S. R., Moe, M., Kratter, K. M., et al. 2023, in Astronomical Society of the Pacific Conference Series, Vol. 534, Protostars and Planets VII, ed. S. Inutsuka, Y. Aikawa, T. Muto, K. Tomida, & M. Tamura, 275, doi: [10.48550/arXiv.2203.10066](https://doi.org/10.48550/arXiv.2203.10066)
- Oliphant, T. 2006, NumPy: A guide to NumPy, USA: Trelgol Publishing. <http://www.numpy.org/>
- Õpik, E. 1924, Publications of the Tartu Astrofizica Observatory, 25, 1
- Perren, G. I., Pera, M. S., Navone, H. D., & Vázquez, R. A. 2023, MNRAS, 526, 4107, doi: [10.1093/mnras/stad2826](https://doi.org/10.1093/mnras/stad2826)
- Raghavan, D., McAlister, H. A., Henry, T. J., et al. 2010, ApJS, 190, 1, doi: [10.1088/0067-0049/190/1/1](https://doi.org/10.1088/0067-0049/190/1/1)
- Reipurth, B., Clarke, C. J., Boss, A. P., et al. 2014, in Protostars and Planets VI, ed. H. Beuther, R. S. Klessen, C. P. Dullemond, & T. Henning, 267, doi: [10.2458/azu_uapress.9780816531240-ch012](https://doi.org/10.2458/azu_uapress.9780816531240-ch012)
- Rekhi, P., Ben-Ami, S., Hallakoun, N., et al. 2024, arXiv e-prints, arXiv:2407.07048, doi: [10.48550/arXiv.2407.07048](https://doi.org/10.48550/arXiv.2407.07048)

- Roberts, J. D., Pinsonneault, M. H., Johnson, J. A., et al. 2024, *MNRAS*, 530, 149, doi: [10.1093/mnras/stae820](https://doi.org/10.1093/mnras/stae820)
- Rosen, A. L., Offner, S. S. R., Sadavoy, S. I., et al. 2020, *SSRv*, 216, 62, doi: [10.1007/s11214-020-00688-5](https://doi.org/10.1007/s11214-020-00688-5)
- Salpeter, E. E. 1955, *ApJ*, 121, 161, doi: [10.1086/145971](https://doi.org/10.1086/145971)
- Shahaf, S., Bashi, D., Mazeh, T., et al. 2023, *MNRAS*, 518, 2991, doi: [10.1093/mnras/stac3290](https://doi.org/10.1093/mnras/stac3290)
- Shahaf, S., Hallakoun, N., Mazeh, T., et al. 2024, *MNRAS*, 529, 3729, doi: [10.1093/mnras/stae773](https://doi.org/10.1093/mnras/stae773)
- Shahaf, S., & Mazeh, T. 2019, *MNRAS*, 487, 3356, doi: [10.1093/mnras/stz1517](https://doi.org/10.1093/mnras/stz1517)
- Shahaf, S., Mazeh, T., & Faigler, S. 2017, *MNRAS*, 472, 4497, doi: [10.1093/mnras/stx2257](https://doi.org/10.1093/mnras/stx2257)
- Shahaf, S., Mazeh, T., Faigler, S., & Holl, B. 2019, *MNRAS*, 487, 5610, doi: [10.1093/mnras/stz1636](https://doi.org/10.1093/mnras/stz1636)
- Tang, J., Bressan, A., Rosenfield, P., et al. 2014, *MNRAS*, 445, 4287, doi: [10.1093/mnras/stu2029](https://doi.org/10.1093/mnras/stu2029)
- Tremblay, P.-E., Bédard, A., O'Brien, M. W., et al. 2024, *NewAR*, 99, 101705, doi: [10.1016/j.newar.2024.101705](https://doi.org/10.1016/j.newar.2024.101705)
- Tremblay, P.-E., Cummings, J., Kalirai, J. S., et al. 2016, *MNRAS*, 461, 2100, doi: [10.1093/mnras/stw1447](https://doi.org/10.1093/mnras/stw1447)
- van Biesbroeck, G. 1916, *AJ*, 29, 173, doi: [10.1086/104155](https://doi.org/10.1086/104155)
- Van der Swaelmen, M., Boffin, H. M. J., Jorissen, A., & Van Eck, S. 2017, *A&A*, 597, A68, doi: [10.1051/0004-6361/201628867](https://doi.org/10.1051/0004-6361/201628867)
- van der Walt, S., Colbert, S. C., & Varoquaux, G. 2011, *Computing in Science Engineering*, 13, 22, doi: [10.1109/MCSE.2011.37](https://doi.org/10.1109/MCSE.2011.37)
- Virtanen, P., Gommers, R., Oliphant, T. E., et al. 2020, *Nature Methods*, 17, 261, doi: [10.1038/s41592-019-0686-2](https://doi.org/10.1038/s41592-019-0686-2)
- Wagg, T., Breivik, K., Renzo, M., & Price-Whelan, A. M. 2024, arXiv e-prints, arXiv:2409.04543, doi: [10.48550/arXiv.2409.04543](https://doi.org/10.48550/arXiv.2409.04543)
- Wagg, T., Breivik, K., Renzo, M., & Price-Whelan, A. M. 2025, *Journal of Open Source Software*, 10, 7400, doi: [10.21105/joss.07400](https://doi.org/10.21105/joss.07400)
- Yamaguchi, N., El-Badry, K., Rees, N. R., et al. 2024a, *PASP*, 136, 084202, doi: [10.1088/1538-3873/ad6809](https://doi.org/10.1088/1538-3873/ad6809)
- Yamaguchi, N., El-Badry, K., Fuller, J., et al. 2024b, *MNRAS*, 527, 11719, doi: [10.1093/mnras/stad4005](https://doi.org/10.1093/mnras/stad4005)